Title:

Homogenization of Cemented Soil Stiffness and Application to the Study of Arching Effects between Jet-Grouted Columns

Authors:

Chloé ARSON, Assistant Professor, School of Civil and Environmental Engineering, Georgia Institute of Technology, Atlanta, Georgia, USA, Phone: 404 385 0143, Fax: 404 894 2278, chloe.arson@ce.gatech.edu

Benjamin JUGE, M.Sc., Zachry Department of Civil Engineering, Texas A&M University, 3136 TAMU, College Station, Texas, USA, Phone: 979.845.7435, juge.benjamin@gmail.com

Abstract:

This paper presents a study of the effect of jet-grouting on soil stiffness. Several homogenization techniques are tested at the scale of a Representative Elementary Volume to determine the stiffness of a mixture made of sand and grout. (1) The averaging method is employed to compute the mechanical stiffness of grouted soil under the assumption that internal stress is mostly supported by the soil skeleton. (2) A hollow sphere model is proposed to predict stiffness under the assumption that soil grains do not contribute to the mechanical resistance of cemented soil. (3) Eshleby's homogenization scheme is used to model cemented soil stiffness for a dilute distribution of grains embedded in grout. The hollow sphere model gives more flexibility in the description of soil fabric, but does not account for soil grain mechanical properties. Eshelby's technique is attractive, but more work is required to improve the representation of cemented soil fabric, especially the soil grain space distribution in the mixture of sand and grout. Settlements above a tunnel surrounded by two rows of jet-grouted columns are computed using the Finite Element Method. Numerical results for vertical displacements and stress are interpreted with Handy's arching theory.

Keywords:

jet-grouting, cemented soil, stiffness, homogenization, arching, Finite Element Method

1. Introduction

Over the last centuries, the increasing size and number of civil engineering structures amplified constraints imposed on the soil. Piles, slabs and other geotechnical structures were designed in order to transfer large stresses in a more efficient way. In certain cases, a combination of improper soils and important loads made those structures insufficient. Ground improvement techniques are aimed at improving hydraulic and mechanical properties of a defined soil mass, either by changing the ground fabric (e.g., compaction and freezing techniques), or by using inclusions (such as mini-piles and sheet piles) to reinforce the soil mass. Jet-grouting consists in injecting a fluid material (such as grout) in the ground, under a high pressure. The aim is to improve the ground resistance (by increasing soil stiffness) and/or to reduce soil permeability. Jet-grouting can be used for tunneling, underpinning and retaining walls (see for instance: Covil & Skinner, 1994; Croce & Flora, 2000; Gazaway & Jasperse, 1992; Katzenbach et al., 1999; Lunardi, 1997; Modoni et al., 2006). The injection technique depends on the ground found in situ and on the material properties that are expected after injection. Models proposed to predict the cemented soil behavior are generally based on constraining assumptions (Croce & Flora, 2000; Modoni et al., 2006) or on empirical considerations (Covil & Skinner, 1994; Gazaway & Jasperse, 1992; Lunardi, 1997). In this paper, the effect of jet-grouting on soil stiffness is investigated at two scales. First, several homogenization techniques are tested at the scale of a Representative Elementary Volume (REV) to determine the stiffness of a mixture made of sand and grout. The Finite Element Method (FEM) is then used to illustrate the development of arching effects between two rows of jet-grouted columns. The objective of the numerical study is to assess the performance of jet-grouting to reduce surface settlements above a tunnel, as a possible alternative to other improvement techniques such as geotextiles (Tahmasebipoor et al., 2012). A row of jet-grouted columns is placed on each side of the tunnel. Handy's arching theory is used to interpret settlements and vertical stresses computed numerically, for various cemented soil elastic moduli and various row spacings.

2. Homogenization of the elastic properties of the injected ground

Several average and homogenization techniques are reviewed and discussed herein, in order to deduce cemented soil elastic properties from the mechanical parameters of the grout and the original soil (before injection). The REV considered for homogenization is the domain around the borehole used for injection, extending up to the grout penetration distance. First, the averaging method is employed to compute the mechanical stiffness of grouted soil under the assumption that internal stress is mostly supported by the soil skeleton. Second, a hollow sphere model is proposed to predict stiffness under the assumption that soil grains do not contribute to the mechanical resistance of cemented soil. Lastly, Eshleby's homogenization scheme is used to model cemented soil stiffness under the assumption that both the grains and the grout contribute to mechanical resistance, for a dilute distribution of grains (assumed to be dispersed close to the injection well).

2.1. Averaging Method – Mechanical Resistance from Soil Grains

In the following averaging model, it is assumed that soil skeleton plays the most important role in cemented soil's mechanical resistance. Grains are assumed to be spheres of equal dimensions, assembled in a hexagonal close packing arrangement. For this geometric configuration, the volumetric fraction of the soil grains is 0.74, and the stiffness tensor of cemented soil is averaged as:

$$\mathbf{C} = 0.26\,\mathbf{C^g} + 0.74\,\mathbf{C^s} \tag{1}$$

in which $\boldsymbol{C^g}$ and $\boldsymbol{C^s}$ are the stiffness tensors of the grout and the soil grains, respectively. Cemented soil compressive strength can be calculated from Eq.(1), for known values of $\boldsymbol{C^g}$ and $\boldsymbol{C^s}$ published in the case studies listed in Table 1. In general, grout and soil Young's moduli are provided by the authors, but Poisson's ratio is not. In the absence of reference data, Poisson's ratio is taken equal to 0.25 for both the grout and the soil. Compressive strength is then deduced from $\boldsymbol{C}$ by assuming that the yield limit of cemented soil in compression is reached for an axial deformation of 0.0025 (this is the value commonly adopted for concrete).

The compressive strengths computed by the model are compared to the reference compressive strengths published in the case studies for the same soil and grout. Fig.1 shows that the relative error generally lies between 1% and 2%, and can be up to 6%. In half of the cases studied, the relative error

is less than 0.1% (almost 0 on the plot). The model seems to be more accurate for low compressive strengths (less than 10MPa). Discrepancies are attributed to the strong assumption made on the geometry of the assembly of soil grains. A more realistic modeling framework would account for particles dislodging due to grout injection.

2.2. Hollow Sphere Model – Mechanical Resistance from the Grout

Now, another extreme case is examined: cemented soil mechanical stiffness is assumed to result from grout mechanical properties only. A hollow sphere model is adopted, to allow studying grain arrangement in the mixture constituted of grout and soil grains. Grains are considered as void inclusions embedded in a grout matrix. Accordingly, the grouted soil is considered as a porous medium constituted of a grout matrix and void pores. The simplest approach consists in considering the REV of cemented soil as one hollow sphere. The sphere cavity represents the fictitious pore space (representing soil grains), and the solid shell represents the solid matrix (made of grout). If the hollow sphere REV is subjected to isotropic stress and strain conditions, the macroscopic bulk modulus of the hollow sphere (k_{hs}) writes (Dormieux et al., 2006):

$$k_{hs} = k_c \frac{4\mu_c (1-\varphi)}{3\varphi k_c + 4\mu_c} \tag{2}$$

in which k_c and μ_c are the bulk and shear moduli of grout, respectively. φ is the porosity of the homogenized medium (representing the volumetric fraction of the sand grains in the cemented soil REV). The separation-of-scale condition required by the theory of homogenization (Nemat-Nasser & Hori, 1993) imposes that the dimension of the pores (inner hollow sphere radius) should be at least three orders of magnitude less than the dimension of the REV (external hollow sphere radius). The basic hollow sphere model is thus only valid for very low porosity media, which is not satisfactory in the present case. Following the approach of Hashin, the REV is considered as an assembly of hollow spheres (Fig.2.a). The inner radius of each hollow sphere is small enough compared to the REV size to satisfy the separation-of-scale requirement (Dormieux et al., 2006). Noting A_i the inner radius of the *i-th* hollow sphere, the porosity of the REV is equal to:

$$\varphi = \frac{\sum_i \frac{4\pi}{3}\left(A_i\right)^3}{V_{REV}} = f\alpha \tag{3}$$

in which V_{REV} is the volume of the REV (Fig.2.b). α is the volume fraction of hollow spheres in the REV (Fig.2.c). Noting B_i the external radius of the *i-th* hollow sphere, and introducing the ratio $x_i = \left(A_i / B_i\right)^3$, the parameter f is the smallest value of ratios $(x_i)_i$ that ensures that all hollow spheres are contained in the REV without overlapping. In other words, for a given set of pores of sizes $\left(A_i\right)_i$, the maximum volume that can be occupied by non-overlapping hollow spheres within the REV is obtained by a set of hollow spheres of external radii $B_i = A_i f^{1/3}$.

The theorem of minimum complementary energy is used to compute a lower bound for the macroscopic bulk modulus of the REV (k_{hom}). According to Dormieux et al. (2006):

$$\frac{1}{k_{\text{hom}}} \le \frac{\alpha}{k_{hs}} + \frac{1-\alpha}{k_c} \tag{4}$$

Using a lower bound to predict the properties of the ground improved by jet-grouting is a conservative approach. In general, k_c, μ_c are known (chosen by the engineer). φ is the volume fraction of the solid grains in cemented soil. It can be determined by comparing the weight of a grout sample (with no soil in it) to the weight of a cemented soil sample after mixing. Assuming that the problem is one-dimensional (radial distribution of stress and strain around the nozzle), Eq.(2) can be used to get k_{hs}. The remaining unknown in Eq.(4) is α, which can be determined if f is known (Eq.(3)). A calibration process is proposed to relate f to k_{hom}.

Nine case studies reported in published articles (Covil & Skinner, 1994; Fang et al., 2004; Gyorgy et al., 1990; Nikbakhtan & Osanloo, 2009; Pellegrino & Adams, 1996; Pichler et al., 2003 & 2004; Shibazaki, 1997; Welsh & Burke, 1991) were used to get reference values for the cemented soil bulk modulus (k_{hom}) with the corresponding grout Young's modulus. Each case study thus provided a reference value of k_{hom} for a given value of k_c. In the absence of value for the grain volumetric fraction after jet-grouting, the value of the porosity of the assembly of hollow spheres was taken equal

to $\varphi = 0.26$ (low volume fraction of grains after injection and mixing). A standard value was chosen for the grout Poisson's ratio (0.25). Inputs were thus: k_c, μ_c, φ. f was adjusted iteratively to ensure that the lower bound computed from Eq.(4) equals the reference value of k_{hom} with less than 3% of error. The variations of f with k_{hom} are plotted in Fig.3. f varies between 0 and 1 for a small range of values of k_{hom}. In other words, there is no typical value of f for typical values of k_{hom}. It is thus impossible to set f as a fixed model parameter.

2.3. Eshelby's Model – Mechanical Resistance from both the Grains and the Grout

The last homogenization technique investigated in this paper accounts for the mechanical properties of both the soil grains and the grout, and allows controlling the density of inclusions (soil grains) in the grout matrix. Assuming that the domain under study is made of a single ellipsoidal inclusion Ω embedded in a matrix $\mathbf{M}$, the stress field in the domain can be written as (Nemat-Nasser & Hori, 1993):

$$\boldsymbol{\sigma} = \begin{cases} \mathbf{C} : \left(\boldsymbol{\varepsilon}^0 + \boldsymbol{\varepsilon}^d \left(\mathbf{x} \right) \right) \text{ in M} \\ \mathbf{C}^{\boldsymbol{\Omega}} : \left(\boldsymbol{\varepsilon}^0 + \boldsymbol{\varepsilon}^d \left(\mathbf{x} \right) \right) \text{ in } \boldsymbol{\Omega} \end{cases} \tag{5}$$

in which $\boldsymbol{\varepsilon}^0$ is the uniform far-field strain prescribed at the boundary of the domain, and $\boldsymbol{\varepsilon}^d \left(\mathbf{x} \right)$ is the disturbance strain field caused by the presence of the inclusion Ω in the domain. An "equivalent homogeneous solid" is defined as the solid of stiffness $\mathbf{C}$ that has the same strain and stress fields as the actual heterogeneous solid made of a matrix (stiffness $\mathbf{C}$) and an inclusion (stiffness $\mathbf{C}^{\boldsymbol{\Omega}}$), under the same stress and strain boundary conditions. Because the actual inclusion is assumed to have a stiffness tensor $\mathbf{C}$ (instead of $\mathbf{C}^{\boldsymbol{\Omega}}$), a correction needs to be made to compute the strain field in the inclusion:

$$\boldsymbol{\sigma} = \begin{cases} \mathbf{C} : \left(\boldsymbol{\varepsilon}^0 + \boldsymbol{\varepsilon}^d \left(\mathbf{x} \right) \right) \text{ in M} \\ \mathbf{C} : \left(\boldsymbol{\varepsilon}^0 + \boldsymbol{\varepsilon}^d \left(\mathbf{x} \right) - \boldsymbol{\varepsilon}^* \left(\mathbf{x} \right) \right) \text{ in } \boldsymbol{\Omega} \end{cases} \tag{6}$$

$\boldsymbol{\varepsilon}^* \left(\mathbf{x} \right)$ is called the eigenstrain, and is related to the far-field and disturbance strain fields by:

$$\boldsymbol{\varepsilon}^0 + \boldsymbol{\varepsilon}^d(\mathbf{x}) = \mathbf{A}^{\boldsymbol{\Omega}} : \boldsymbol{\varepsilon}^*(\mathbf{x}), \quad \mathbf{A}^{\boldsymbol{\Omega}} = \left(\mathbf{C} - \mathbf{C}^{\boldsymbol{\Omega}}\right)^{-1} : \mathbf{C} \tag{7}$$

Eshelby proved that if the matrix is homogeneous, linearly elastic, and infinitely extended, and if Ω is an ellipsoid, then $\boldsymbol{\varepsilon}^*(\mathbf{x})$ and $\boldsymbol{\varepsilon}^d(\mathbf{x})$ are uniform in Ω and the relationship between $\boldsymbol{\varepsilon}^*(\mathbf{x})$ and $\boldsymbol{\varepsilon}^d(\mathbf{x})$ is linear (Nemat-Nasser & Hori, 1993):

$$\boldsymbol{\varepsilon}^d(\mathbf{x}) = \boldsymbol{\varepsilon}^d = \mathbf{S}^{\boldsymbol{\Omega}} : \boldsymbol{\varepsilon}^* = \mathbf{S}^{\boldsymbol{\Omega}} : \boldsymbol{\varepsilon}^*(\mathbf{x}) \tag{8}$$

$\mathbf{S}^{\boldsymbol{\Omega}}$ is called Eshelby's tensor, and only depends on the geometry of the ellipsoidal inclusion. Reference values for basic geometric shapes may be found in (Nemat-Nasser & Hori, 1993). In the following, it is assumed that the space distribution of soil grains (inclusions) is dilute, since the REV considered for homogenization is located in the vicinity of the borehole, where soil grains are dispersed due to high-pressure grout injection. Therefore inclusions do not interact, and each individual inclusion can be considered as a solid embedded in an infinitely extended matrix. Eshelby's model can thus be used (Nemat-Nasser & Hori, 1993) in order to determine the homogenized stiffness tensor ($\mathbf{C}^{\mathbf{hom}}$) of a dilute distribution of N ellipsoidal soil grains, embedded in a grout matrix (of stiffness $\mathbf{C}$):

$$\mathbf{C}^{\mathbf{hom}} = \mathbf{C} : \left[\mathbf{I}^{(4)} - \sum_{j=1}^{N} f_j \left(\mathbf{A}^j - \mathbf{S}^j\right)^{-1}\right] \tag{9}$$

in which $\mathbf{I}^{(4)}$ is the fourth-order identity tensor, and $\mathbf{C}^j$, $\mathbf{S}^j$ and f_j are respectively the stiffness tensor, Eshelby's tensor and the volume fraction of the j-th inclusion. If all inclusions (soil grains) have the same geometric and elastic properties:

$$\forall j, \quad \mathbf{A}^j = \mathbf{A}^{\boldsymbol{\Omega}} \quad \text{and} \quad \mathbf{S}^j = \mathbf{S}^{\boldsymbol{\Omega}} \tag{10}$$

and Eq.(9) writes:

$$\mathbf{C}^{\mathbf{hom}} = \mathbf{C} : \left[\mathbf{I}^{(4)} - \left(\mathbf{A}^{\boldsymbol{\Omega}} - \mathbf{S}^{\boldsymbol{\Omega}}\right)^{-1} \sum_{j=1}^{N} f_j\right] = \mathbf{C} : \left[\mathbf{I}^{(4)} - f_{tot}\left(\mathbf{A}^{\boldsymbol{\Omega}} - \mathbf{S}^{\boldsymbol{\Omega}}\right)^{-1}\right] \tag{11}$$

in which f_{tot} represents the volume fraction of all inclusions (soil grains) contained in the Representative Elementary Volume. Eshelby's model has been tested by comparing the compressive strength of cemented soil computed according to Eq.(11) (with a yield axial deformation of 0.0025

and a dilute distribution of ellipsoidal soil grains) to reference compressive strengths measured by other research teams for the same soil and grout materials (Table 1). Fig.4 shows that the relative error is less than 0.1% (almost 0 on the plot) for half of the cases studied, and never exceeds 3%. The model predictions are accurate in compression, but more reference data is necessary to test the performance of Eshelby's model to predict shear strength.

It is worth noticing that the prediction of cemented soil compressive strength is accurate both under the assumption of close grain packing (averaging method) and under the assumption of dilute grain distribution (Eshelby's model). Since the present study focuses on coarse-grained soils (Tab.1), it is expected that the two approaches would lead to different shear resistances. If the volume fraction of grain inclusions is large compared to the volume fraction of grout, poor grain bonding will yield a low shear resistance. If grains a sparsely distributed in a grout matrix, the high grout content will increase cemented soil cohesion and shear resistance. Future research work will aim to:

- account for the elastic properties of both the grout and the soil (impossible with the hollow sphere model),
- determine relevant geometric parameters to calibrate the homogenized cemented soil model (impossible with the hollow sphere model and the averaging technique),
- improve the representation of cemented soil fabric in the model, especially the soil grain space distribution in cemented soil (limitation of the three models studied in this paper).

3. Arching Effect between Two Rows of Jet-Grouted Columns

The purpose of the following section is to study the performance of jet-grouting to reduce surface settlements by arching effect. A series of simulations is performed with PLAXIS Finite Element software to evaluate arching effects between two rows of jet-grouted columns placed on both sides of a tunnel. Numerical results are interpreted and discussed in light of Handy's arching theory, which was initially proposed to compute stress distributions in soil behind frictional walls (Handy, 1985).

3.1. Arching Effect Between Two Frictional Walls: Handy's Model

Handy's theory assumes that between two frictional walls separated by a distance $2L$, the principal directions of stress developed in the soil reorient in such a way that the locus of all material points having the same principal stresses forms a catenary (Fig.5), the equation of which is given by (Handy, 1985):

$$z = a\cosh\left(\frac{x}{aL}\right) \tag{12}$$

in which a is a material parameter, and z is the depth of the point considered ($z = 0$ at the ground surface, axis oriented upward). Noting P the point of the catenary at mid-distance between the two walls, x is the distance between P and the point considered.

The major principal stress at P ($\sigma_1(P)$) is equal to the vertical stress at that point:

$$\sigma_1(P) = \sigma_v(P) \tag{13}$$

On the contrary, due to the reorientation of stress induced by friction at the walls, the major principal stress at the point of intersection of a wall with the catenary (noted S) is not equal to the vertical stress at that point:

$$\sigma_1(S) \neq \sigma_v(S) \tag{14}$$

At S, vertical stress is induced by the weight of the upper soil layer:

$$\sigma_v(S) = -\gamma_{soil} z_S \tag{15}$$

In the absence of arching effects, the catenary is actually a horizontal line, and the vertical stress at P can be computed with Eq.(15). On the contrary, if friction at the wall surfaces induces an arching

effect, the vertical stress in the middle of this horizontal line cannot be computed from the weight of the upper soil layer, and as a result:

$$\sigma_v(P) \neq -\gamma_{soil} z_P \tag{16}$$

To compute $\sigma_v(P)$, it is necessary to determine $\sigma_1(P)$. According to Handy's theory:

$$\sigma_1(P) = \sigma_1(S) \tag{17}$$

At S, shear failure has occurred and the current shear stress can be determined by using Mohr-Coulomb's criterion (Handy, 1985):

$$\tau(S) = c + \sigma_v(S)\tan\phi \tag{18}$$

in which c and ϕ are the soil's cohesion and friction angle, respectively. The combination of Eq.(15) and Eq.(18) provides one point on Mohr's circle (noted M). The perpendicular to the failure envelope at that point intersects the horizontal axis at the center of Mohr's circle (noted C). CM is the radius of Mohr's circle for a soil element located at material point S. Using Mohr's circle, one can deduce $\sigma_1(S)$, and thus $\sigma_v(P)$ (according to Eq.(13, 17-18)). In addition, the depth of point P as compared to the depth of point S is given by the equation of the catenary (Eq.(12)):

$$z_P = z_S - a\cosh\left(\frac{1}{a}\right) \tag{19}$$

In order to illustrate the effects of arching predicted by Handy's theory, vertical stress was computed at mid-distance between two frictional walls, for various wall spacings ($2L$). Stress values are plotted against depth in Fig.6. The soil considered was a sand ($c = 0$) having a specific weight $\gamma_{soil} = 20\text{kN/m}$ and a friction angle $\phi = 20°$. According to Handy (1985), $a = 1.532$ for $\phi = 20°$. The space distribution of vertical stress shows a discontinuity at z_P. Above P, vertical stress is computed from the specific weight of the upper soil layer. Below P, arching tends to reduce vertical stress: vertical stress is equal to the sum of $\sigma_v(P)$ and the vertical stress induced by the specific weight of the soil below P, which is less than the vertical stress induced by the total weight of the upper layers above and below P.

3.2. Arching Effects Observed Between Two Rows of Cemented soil Columns

PLAXIS Finite Element software is used to simulate arching effects occurring around a tunnel constructed in a soil mass reinforced by two rows of jet-grouted columns. The mechanical properties of the materials used in the simulation are listed in Table 2. Note that the Young's modulus of cemented sand is given different values in the parametric study presented in the following. All the other constitutive parameters (Poisson's ratio, cohesion, friction angle) are assumed to be the same in sand and cemented soil, in order to focus the discussion on the influence of the mechanical stiffness of jet-grouted columns in the development of arching.

The geometry and boundary conditions are shown in Fig.7. Displacements were fixed at the bottom of the domain, and horizontal displacements were blocked on lateral boundaries. There was no shear force along the lateral boundaries. Neumann boundary conditions were applied at the top (details are provided for each simulation presented in the following). Triangular elements were used. The typical element size was 2 meters in the far field, and mesh was refined close to the tunnel wall (element size decreased by a factor of 5). The numerical model was designed in plane strain, which implies that the two rows of jet-grouted columns were modelled as two infinitely long solid walls.

Fig. 8 illustrates the effects of arching observed for a row spacing of 13 meters, in which the top boundary was free of stress. To illustrate the shape of the distribution of vertical settlements, a downward vertical load of 1kN/m was applied between the two "walls" representing the rows of columns. This preliminary test illustrates the role of friction at the walls, and the subsequent arching effects. Realistic loading conditions are used in the following, to compare the development of arching for different design strategies (e.g. column spacing, stiffness of cemented soil).

3.3. Parametric Studies

A vertical load of 20kN/m was applied on the full length of the top boundary, and arching effects were studied for various cemented soil elastic properties and column spacings. The soil properties and the bottom and lateral boundary conditions were the same as in the case shown in Fig.8. The results obtained for a cemented soil modulus of 3 GPa and 15 GPa are illustrated in Fig.9(a) and Fig.9(b), respectively. Vertical displacements follow the expected trends: the stiffer the cemented soil, the

larger the stress developed in the jet-grouted columns, and, in particular, the larger the shear stress at the interface between the columns and the soil. According to Handy's theory, the higher the shear stress induced by friction, the larger arching effects and the less important settlements.

The simulation was run with a cemented soil modulus of 3GPa, for various column spacings (Fig.10). The results illustrate the discontinuity of vertical stress at the yield locus. The numerical predictions follow the trends expected from Handy's theory: between the two rows of jet-grouted columns, the location of the points where shear failure occurred has the shape of a catenary.

4. Conclusion

This paper presents a study of the effect of jet-grouting on soil stiffness. Several homogenization techniques are tested at the scale of a Representative Elementary Volume. (1) The averaging method is employed to compute the mechanical stiffness of grouted soil under the assumption that internal stress is mostly supported by the soil skeleton. (2) A hollow sphere model is proposed to predict stiffness under the assumption that soil grains do not contribute to the mechanical resistance of cemented soil. (3) Eshleby's homogenization scheme is used to model cemented soil stiffness for a dilute distribution of grains embedded in grout. The hollow sphere model gives more flexibility in the description of cemented soil fabric, but does not allow accounting for soil grain mechanical properties (grains are considered as void inclusions). Moreover, it is impossible to characterize the size distribution of hollow spheres by a unique model parameter for standard soil and grout properties in usual jet-grouting conditions. Eshelby's technique is attractive, but more work is required to improve the representation of cemented soil fabric in the model, especially the soil grain space distribution in cemented soil. In addition to soil strengthening, jet-grouting is expected to improve soil bearing capacity due to arching effects. Arching is caused by the reorientation of stress in the soil, due to the friction developed at the interface between cemented soil columns and the soil. To illustrate this phenomenon, settlements above a tunnel surrounded by two rows of cemented soil columns were computed using a plane strain Finite Element model. This is an original application of jet-grouting for ground improvement purposes. The distribution of vertical stress above the tunnel shows a discontinuity at the depth where stress reorients due to arching. This is in agreement with the catenary-shaped yield locus hypothesized in Handy's arching theory. On a short-term perspective, the homogenization scheme will be improved to better account for cemented soil fabric. On a longer-term perspective, the approach presented in this paper is expected to improve the prediction of arching effects in embankments supported by grouted columns.

References

Covil, C.S. and Skinner, A.E. (1994). "Jet-grouting: a review of some of the operating parameters that form the basis of the jet grouting process", in: *Grouting in the Ground*, Thomas Telford, London, pp. 605-629.

Chiari, A. and Croce, P. (1991). "Some Limits to the Use of Jet-Grouting", *Proc. 4th International Conference on Piling and Deep Foundations*, Stresa, Italy, April 7-12, 1991, Vol.1, pp. 201-204

Croce, P. and Flora, A. (2000). "Analysis of single-fluid jet grouting". *Géotechnique*, Vol. 50, pp. 739-748.

Dormieux, L., Kondo, D. and Ulm, F.-J. (2006). *Microporomechanics*. John Wiley & Sons, Chichester, England

Fang YS, Kuo LY, and Wang DR. (2004). "Properties of cemented soil stabilized with jet grouting", *Proc. 14th International Offshore and Polar Engineering Conference,* International Society of Offshore and Polar Engineers, Toulon, France, May 23-28, 2004, Vol. 2, pp. 696-702

Gazaway, H.N. and Jasperse, B.H. (1992). "Jet Grouting in Contaminated Soils", in: Grouting, Soil Improvement and Geosynthetics, *Geotechnical Special Publication*, No. 30, pp. 206-214.

Gruner, L.B. (1999). "Jet-Grouting in Cohesive Soils", in: Geo-Engineering for Underground Facilities, *Geotechnical Special Publication*, No. 90, pp. 1016-1026

Gyorgy, P., Hajnal, I. and Zsigmondi A. (1990). "Foundation reinforcing of surrounding buildings around construction sites in urban areas by using jet grouting technology", *Proceedings of the 9th Danube-European Conference on Soil Mechanics and Foundation Engineering*, Budapest, Hungary, October 2-5, 1990, pp. 449-454

Handy, R.L. (1985). "The Arch in Soil Arching". *Journal of Geotechnical Engineering, ASCE*, Vol. I11, No. 3, pp. 302-318

Katzenbach, R., Iagolnitzer, Y. and Moormann, C. (1999). "New experimental results and sites experiences on grouting techniques", *Geotechnical Engineering for Transportation Infrastructure*, Vol.1-3: Theory and Practice, Planning and Design, Construction and Maintenance, pp. 1419-1431

Kauschinger, J.L., Perry, E.B. and Hankour R. (1992). "Jet Grouting: State-of-the-practice", in: Grouting, Soil Improvement and Geosynthetics, *Geotechnical Special Publication*, No. 30, pp. 169-181

Lunardi, P. (1997). "Ground Improvement by Means of Jet-Grouting", *Proceedings of the ICE*, Vol. 1, No. 2, pp. 65-85.

Modoni, G., Croce, P. and Mongiovi, L. (2006). "Theoretical Modeling of Jet-Grouting", *Géotechnique*, Vol. 56, No. 5, pp. 335-347.

Nemat-Nasser, S. and Hori, M. (1993). *Micromechanics: Overall Properties of Heterogeneous Materials*. North-Holland. Amsterdam, The Netherlands

Nikbakhtan, B. and Osanloo, M. (2009). "Effect of grout pressure and grout flow on soil physical and mechanical properties in jet grouting operations", *International Journal of Rock Mechanics & Mining Sciences*, Vol. 46, No. 3, pp. 498-505

Pellegrino, G. and Adams, DN. (1996). "The use of jet grouting to improve soft clays for open face tunnelling", in: Geotechnical aspects of underground construction in soft ground*, Proceedings of the international symposium on geotechnical aspects of underground Construction in Soft Ground*, Balkema puplishers, London, England, April 15-17, 1996, pp. 423-428

Pichler, C., Lackner, R., Martak, L. and Mang, H.A. (2004). "Optimization of jet-grouted support in NATM tunneling", *International journal for numerical and analytical methods in geomechanics*, Vol. 28, No. 7-8, pp. 781-796

Pichler, C., Lackner, R., Spira, Y. and Mang, H.A. (2003). "Thermochemomechanical Assessment of Ground Improvement by Jet Grouting in Tunneling", *Journal of Engineering Mechanics*, Vol. 129, No. 8, pp. 951-962

Shibazaki, M. (1997). "State of the art grouting in Japan ", in Grouting and Deep Mixing, *Proc. 2nd International Conference on Ground Improvement Geosystem*, ICE publishers, Tokyo, Japan, May 14-17, 1997, Vol. 2, pp. 851-867

Tahmasebipoor, A., Noorzad, R., Shooshpasha, E., & Barari, A. (2012). A parametric study of stability of geotextile-reinforced soil above an underground cavity. *Arabian Journal of Geosciences*, *5*(3), 449-456.

Welsh, J.P. and Burke, GK. (1991). "Jet Grouting - Uses for Soil Improvement", in: Geotechnical Engineering Congress 1991, *Geotechnical Special Publication*, Vol. 1&2, No. 27, pp. 334-345

Table 1. Published Case Studies Used as References to Compare Homogenization Techniques.

Case	Reference
1	Kauschinger et al., 1992
2	Pellegrino & Adams, 1996
3	Gruner, 1999
4	Croce & Flora, 2000
5	Pichler et al., 2003
6	Gyorgy et al., 1990
7	Chiari & Croce, 1991
8	Welsh & Burke, 1991
9	Lunardi, 1997
10	Shibazaki, 1997
11	Fang et al., 2004
12	Pichler et al., 2004

Table 2. Properties of the materials studied in the simulations.

Material	Sand	Cemented Sand (jet-grouted columns)	Concrete (tunnel support)
Behavior Model	Mohr-Coulomb	Mohr-Coulomb	Elastic
γ [kN/m^3]	10	14	
w [kN/m^3]			8.4
d [m] – shell thickness			0.35
E [MPa]	80	3000	
EA [MN/m]			14000
EI [MNm]			143
ν	0.3	0.3	0.15
c (cohesion) [Pa]	0	0	
Φ (friction angle) [°]	31	31	
Ψ (dilatancy angle) [°]	0	0	

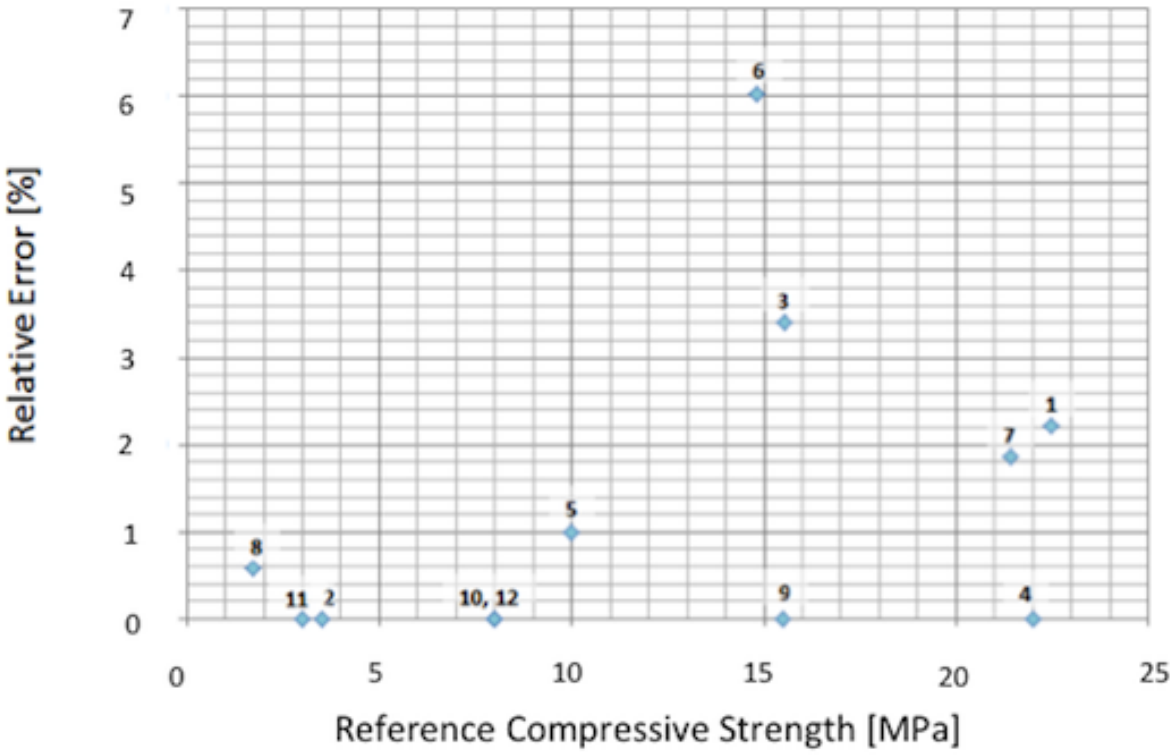
Relative Error [%]
Reference Compressive Strength [MPa]
0
1
2
3
4
5
6
7
0
5
10
15
20
25
6
3
1
7
5
8
11
2
10, 12
9
4

Figure 1:

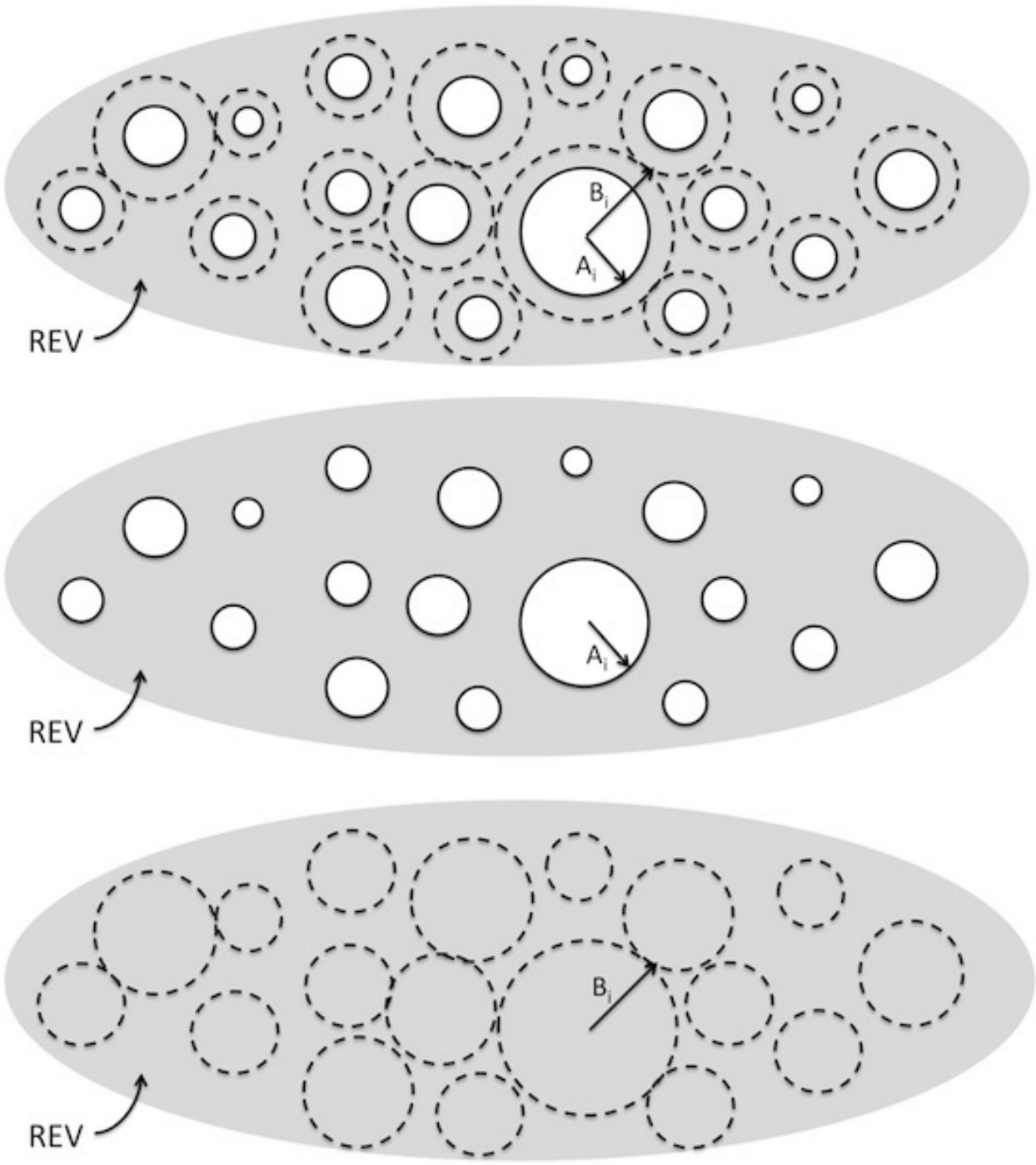

Figure 2:

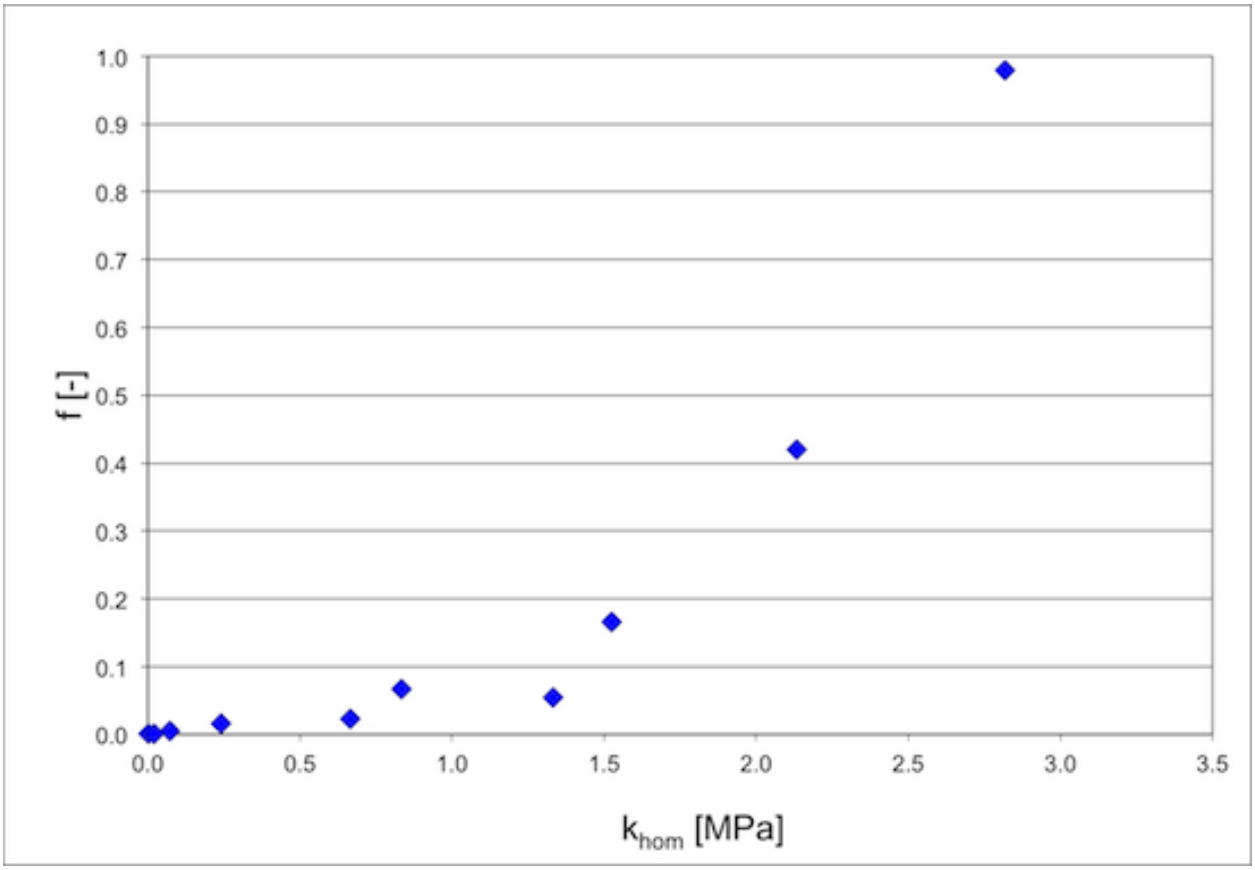

Figure 3:

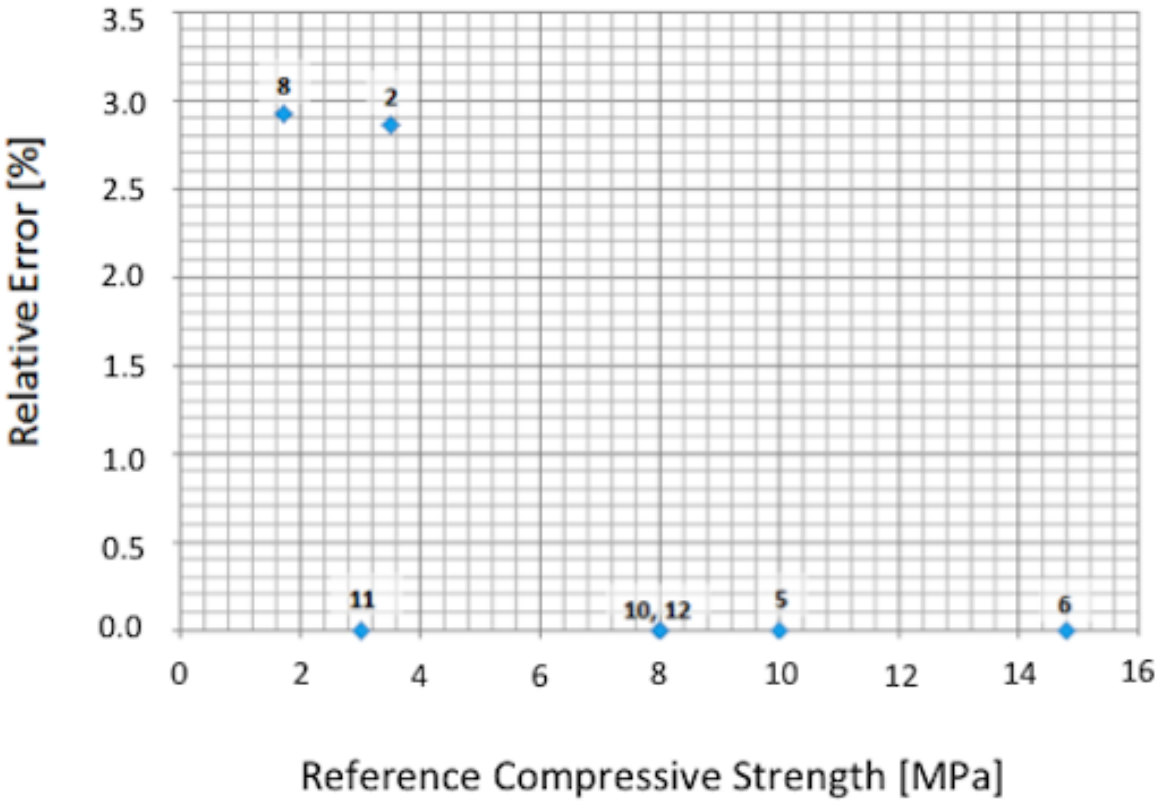
Relative Error [%]
3.5
3.0
2.5
2.0
1.5
1.0
0.5
0.0
0
2
4
6
8
10
12
14
16
8
2
11
10, 12
5
6
Reference Compressive Strength [MPa]

Figure 4:

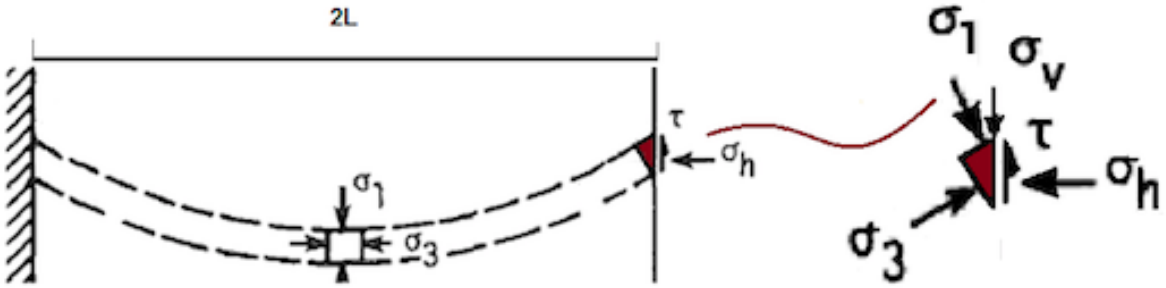

Figure 5:

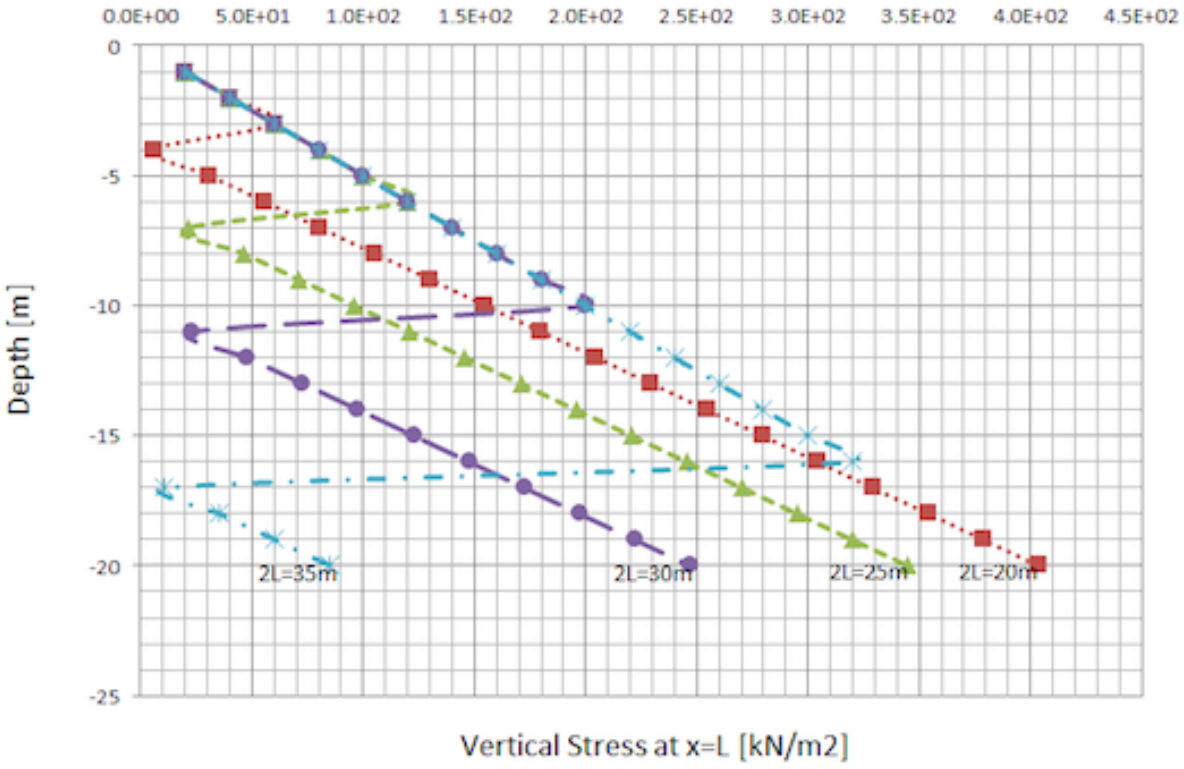
0.0E+00
5.0E+01
1.0E+02
1.5E+02
2.0E+02
2.5E+02
3.0E+02
3.5E+02
4.0E+02
4.5E+02
0
-5
-10
-15
-20
-25
Depth [m]
2L=35m
2L=30m
2L=25m
2L=20m
Vertical Stress at x=L [kN/m2]

Figure 6:

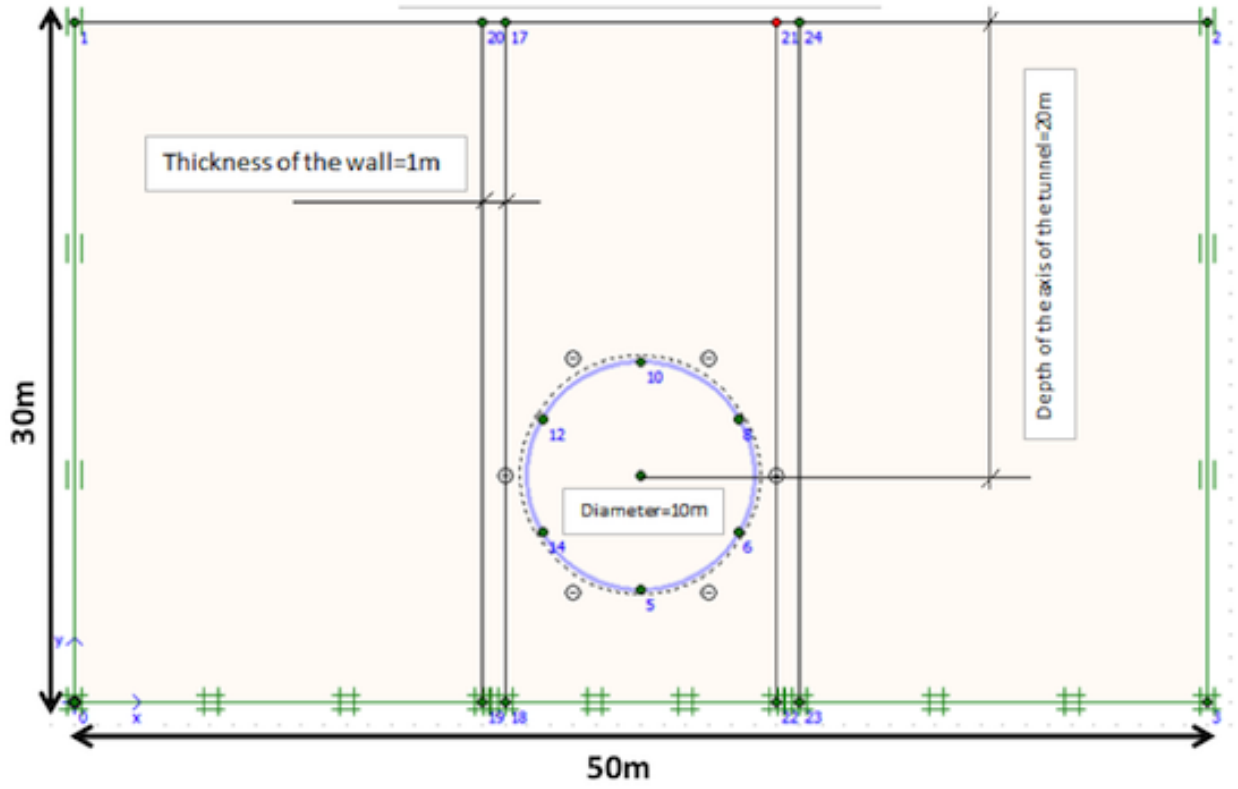
Thickness of the wall=1m
Depth of the axis of the tunnel=20m
Diameter=10m
30m
50m

Figure 7:

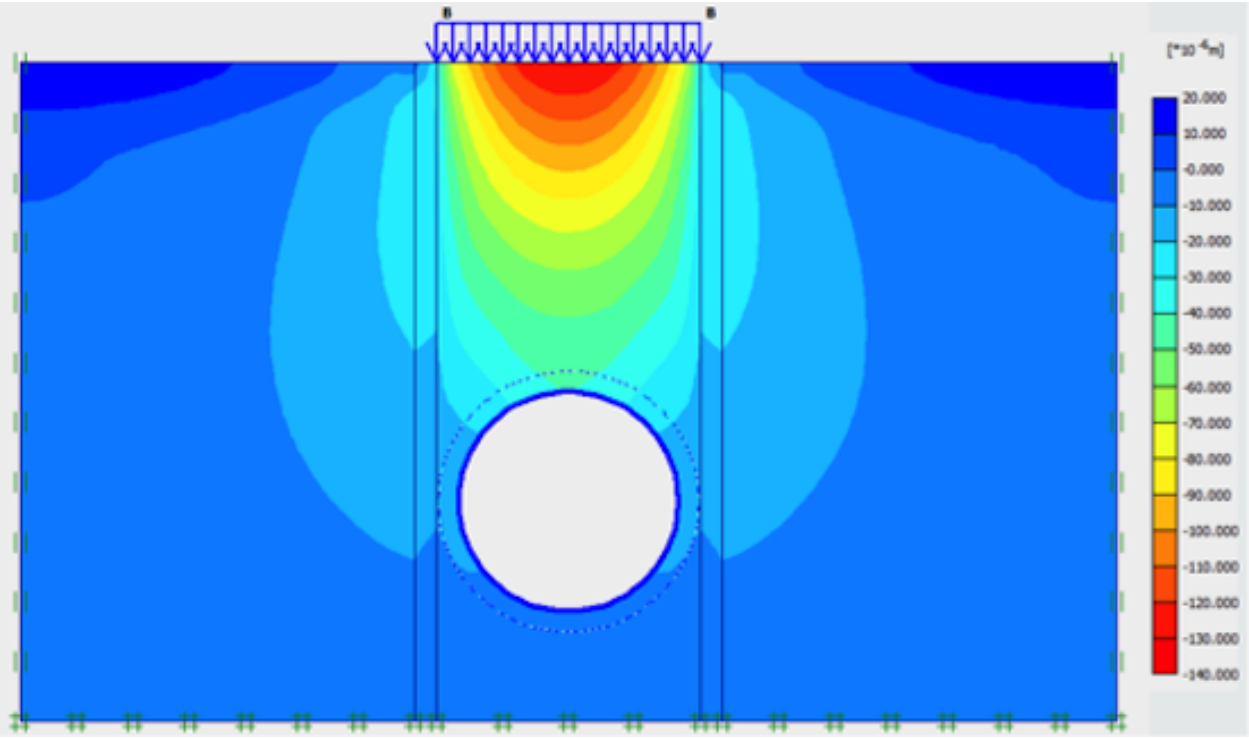
[*10 -4 m]
20.000
10.000
-0.000
-10.000
-20.000
-30.000
-40.000
-50.000
-60.000
-70.000
-80.000
-90.000
-100.000
-110.000
-120.000
-130.000
-140.000

Figure 8:

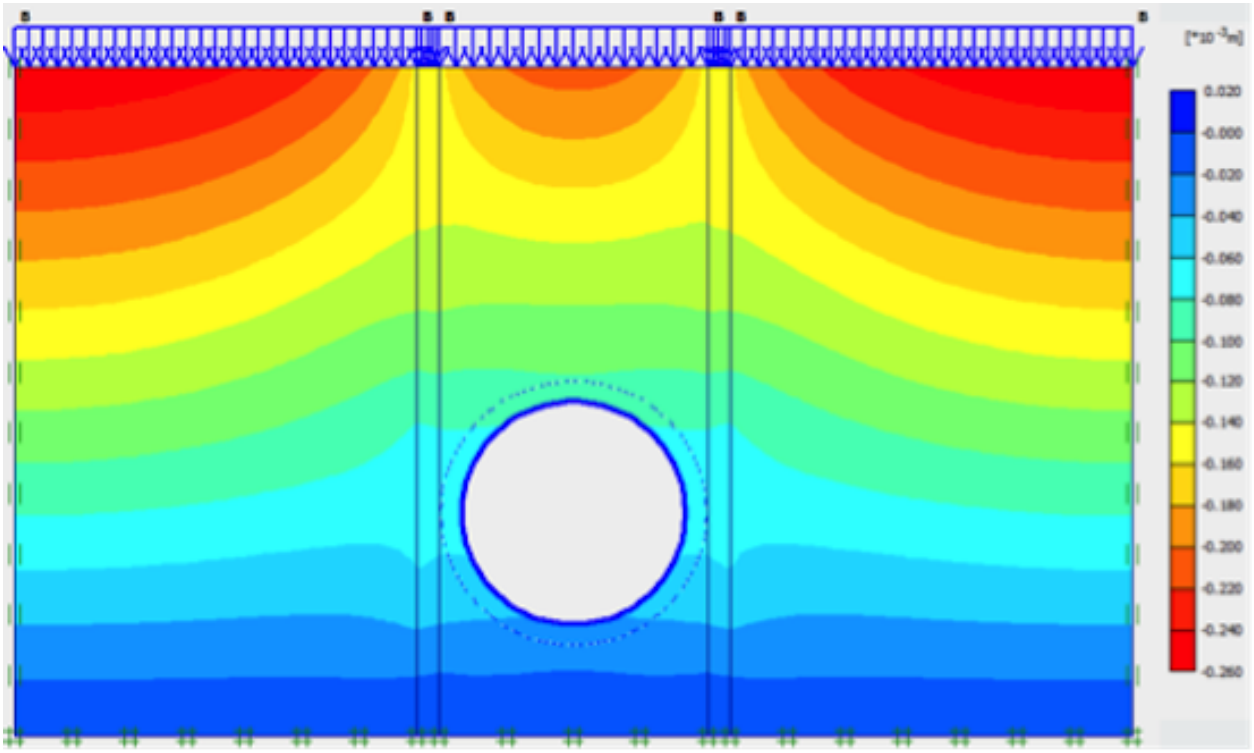
[*10 -3 m]
0.020
-0.000
-0.020
-0.040
-0.060
-0.080
-0.100
-0.120
-0.140
-0.160
-0.180
-0.200
-0.220
-0.240
-0.260

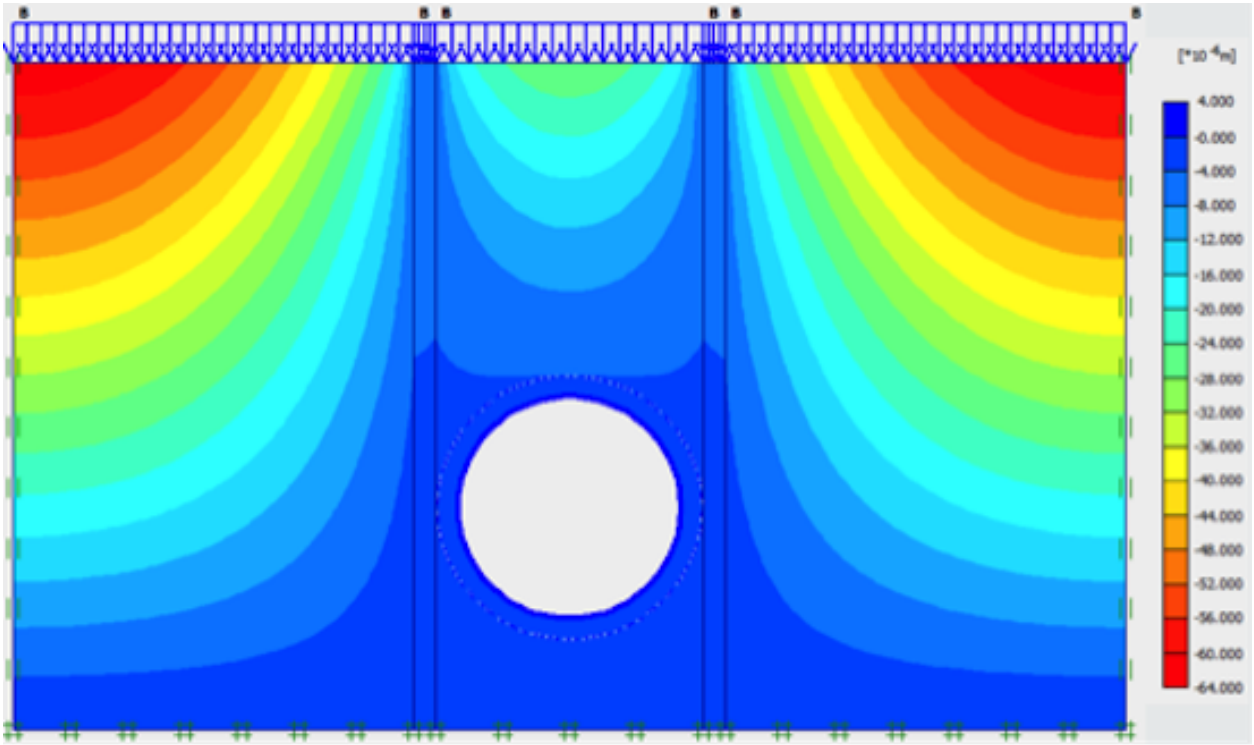
[*10 -6 m]
4.000
-0.000
-4.000
-8.000
-12.000
-16.000
-20.000
-24.000
-28.000
-32.000
-36.000
-40.000
-44.000
-48.000
-52.000
-56.000
-60.000
-64.000

Figure 9:

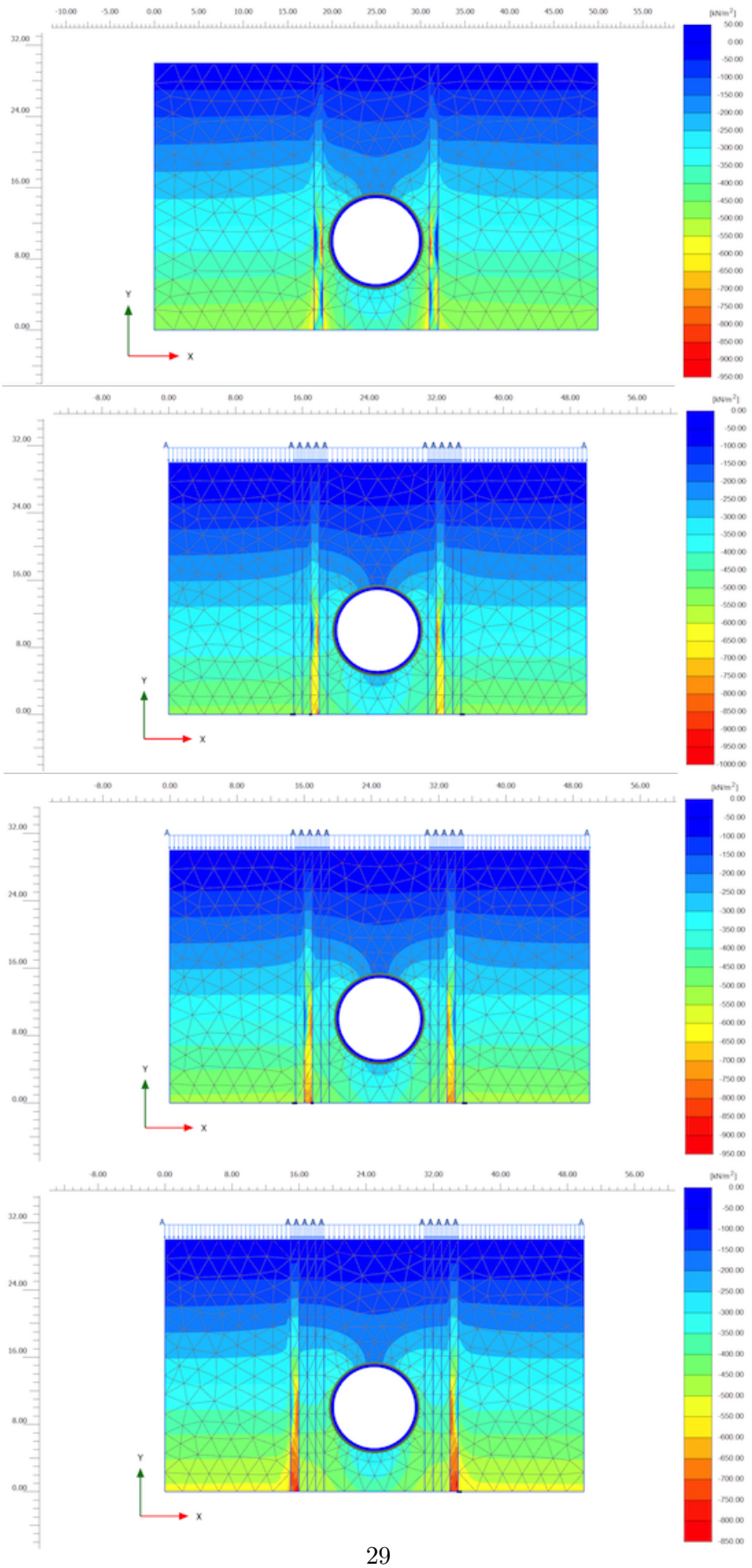
-10.00 -5.00 0.00 5.00 10.00 15.00 20.00 25.00 30.00 35.00 40.00 45.00 50.00 55.00
32.00
24.00
16.00
8.00
0.00
Y
X
[kN/m²]
50.00
0.00
-50.00
-100.00
-150.00
-200.00
-250.00
-300.00
-350.00
-400.00
-450.00
-500.00
-550.00
-600.00
-650.00
-700.00
-750.00
-800.00
-850.00
-900.00
-950.00
-8.00 0.00 8.00 16.00 24.00 32.00 40.00 48.00 56.00
-1000.00

Figure 10: